

RXTE Observations of Cygnus X-1

Broad-Band Spectra and High-Resolution Timing

K. Pottschmidt¹, J. Wilms¹, M.A. Nowak², J.B. Dove³, M.C. Begelman², and R. Staubert¹

¹ Institut für Astronomie und Astrophysik – Astronomie, Waldhäuser Str. 64, D-72076 Tübingen, Germany

² JILA, University of Colorado, Boulder, CO 80309-440, U.S.A.

³ CASA, University of Colorado, Boulder, CO 80309-389, U.S.A.

Abstract. We present results from a 20 ksec RXTE observation of the black hole candidate Cyg X-1. We apply self-consistent accretion disk corona models to these hard state data and show that Comptonization in a spherical corona irradiated by soft photons from an exterior cold disk is able to successfully model the spectrum. We also present the power spectrum, the coherence function, and the time lags for lightcurves from four energy bands. By modeling the high-resolution lightcurves with stochastic linear state space models, we show that the rapid hard state variability of Cyg X-1 can be explained with a single timescale.

1. Introduction

The X-ray emission of galactic black hole candidates (BHCs) displays different “states” characterized by distinct temporal and spectral properties (Esin, McClintock & Narayan, 1997; van der Klis, 1995). Except for occasional transitions to the soft state, Cyg X-1 spends most of its time in the hard state (Fig. 1). It is therefore the prime candidate for evaluating accretion models of this fundamental black hole state.

Since 1996 the Rossi X-ray Timing Explorer (RXTE) provides data from 3 to 200 keV with millisecond time-resolution. In this paper we derive a wide variety of spectral and temporal hard state properties by applying physical accretion disk corona models (ADCs) (Sect. 3) as well as new timing methods (Sect. 4 and 5) to a RXTE hard state observation of Cyg X-1. Whereas ADCs are very successful in explaining the observed spectrum (Dove et al., 1997), a unified model for the hard state accretion also has to take into account the time dependence of the emission. Some of the associated constraints that are provided by the power spectral density, the coherence function, the time lags, and the lightcurve modeling with stochastic processes, are discussed in sections 4 and 5. For further discussion see Nowak et al. (1998, 1999) and Pottschmidt et al. (1998).

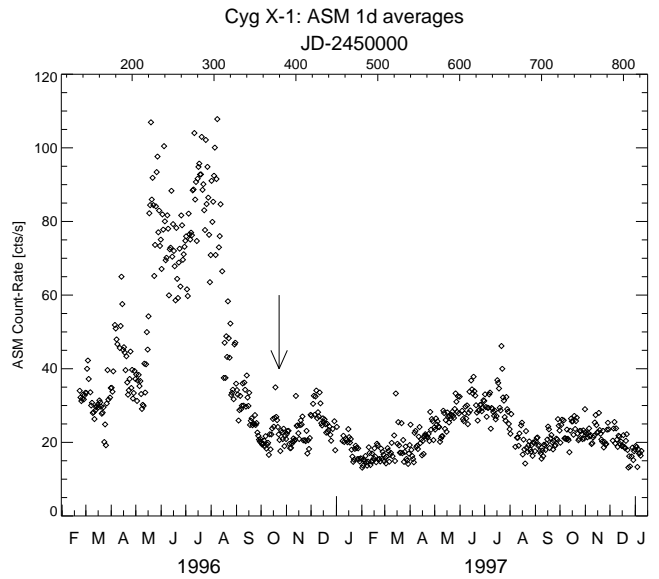


Fig. 1. RXTE-ASM count-rates in the 1.5 to 12 keV band for Cyg X-1 from the beginning of the ASM measurements until 1997 December. The arrow indicates the time of our pointed RXTE observation. The 1996 soft state can be clearly identified by the increased count-rate from 1996 May through August.

2. Data Extraction

RXTE observed Cyg X-1 for a total integrated source time of slightly more than 20 ksec, starting 1996 October 23, briefly after its transition to the hard state (Fig. 1).

We analyzed data from the Proportional Counter Array (PCA) as well as from the High Energy X-ray Timing Experiment (HEXTE). An overview of our data screening procedures and of the RXTE instruments is given by Dove et al. (1998) and Wilms et al. (this volume). For the spectral analysis we used 3 to 30 keV PCA data and 20 to 200 keV HEXTE data. The temporal analysis is based on PCA lightcurves with 1.95 ms resolution from four energy bands with approximately equal count rates ($\mathcal{O}(700\text{--}1000)$ cts s⁻¹ per band). The energy bands are defined in Fig. 3, the total length of the lightcurves was ~ 18 ksec.

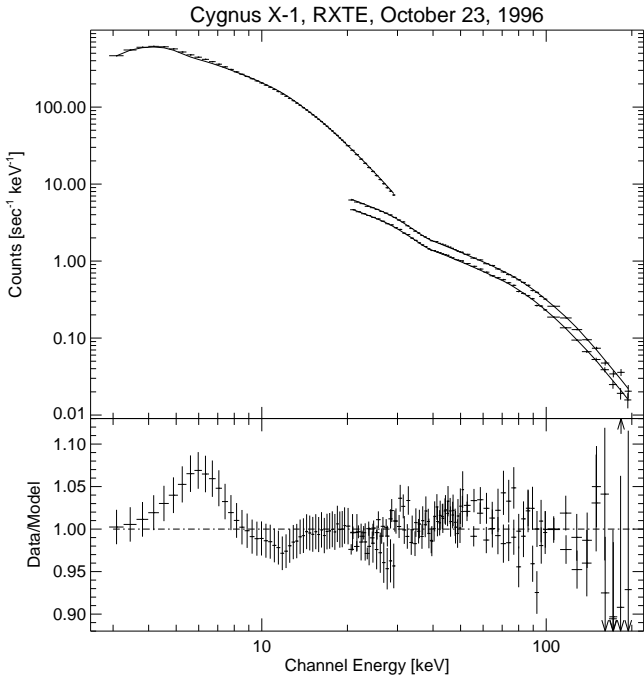


Fig. 2. Fit of the sphere+disk model to the data, indicating good overall agreement between the ADC model and the observations ($\chi^2_{\text{red}} = 1.55$, assuming a systematic error of 2% for the PCA data). The corona has a temperature of $kT = (65.7 \pm 3.3)$ keV and an optical depth of $\tau = 2.1 \pm 0.1$. The seed photons were assumed to come from an accretion disk external to the corona, with a $r^{-3/4}$ temperature profile and an inner accretion disk temperature of 150 eV.

More details on the PCA timing data of this observation are given by Nowak et al. (1999).

3. Spectral Modeling: Self-Consistent Thermal Accretion Disk Corona Models

The BHC hard state spectrum, a power-law with $\Gamma \sim 1.65$, modified by an exponential cutoff with $E_{\text{fold}} \sim 150$ keV is naturally explained by accretion disk corona (ADC) models, i.e., by Comptonization of low-energy seed photons from a cold, geometrically thin accretion disk in a hot, semi-relativistic corona (Titarchuk, 1994). As we explain in more detail in an accompanying paper (Wilms et al., this volume; see also Dove, Wilms & Begelman, 1997; Dove et al., 1997), we have developed an ADC model in which the radiation field, the temperature and opacity of the corona, and the reprocessing of coronal radiation in the accretion disk are calculated self-consistently. The commonly assumed slab geometry where the accretion disk is sandwiched between two coronae is not self-consistent, since the coronal temperatures and opacities are not within the physically allowed range of combinations of these parameters. On the other hand, the

sphere+disk geometry where the seed photons come from an accretion disk external to the inner spherical corona, allows to fit the broad-band spectrum of Cyg X-1 with *one* self-consistent model.

The best-fit sphere+disk spectrum for our RXTE observation is shown in Fig. 2. The deviations between the data and model above 10 keV are consistent with the current calibration uncertainty of the PCA, while the deviation in the iron band between 5 and 10 keV shows the physical simplifications in our model. This does not pose a severe problem to the model since the deviations represent less than 1% of the total flux modeled. The deviation might be due to an underestimation of the covering factor for reflection, e.g., by a possible overlap between the disk and the corona due to the transition from the soft to the hard state two weeks before the observation (cf. Fig. 1). The presence of accretion disk flares (due to disk heating) would also increase the reprocessing observed. Finally, a slight increase in the Fe abundance will also produce the stronger line seen in the data. See Dove et al. (1998) for a discussion of these points, as well as for a presentation of spectral fits using phenomenological “standard” models.

4. Timing: Fourier Methods

4.1. Power Spectral Density

We calculated power spectral densities (PSDs) by dividing the data into contiguous segments of uniform length and computing the Fourier transform $S_j(f)$ of each data segment. The discrete PSD is then given by $\langle |S_j|^2 \rangle$ where the brackets indicate an average over data segments and logarithmic frequency bins (Fig. 3, see also Nowak et al., 1999).

The PSDs show characteristic hard state behavior (cf. Belloni & Hasinger, 1990). For 10^{-3} –100 Hz the rms variability in all bands is about 30%. The PSDs are relatively flat for frequencies from 0.02–0.2 Hz. For higher frequencies, they are roughly described by a steepening, broken power-law with a break at ~ 2 Hz, and typical slopes of -1.0 , and -1.5 , respectively. Note that while there are no strong energy dependences, the high frequency slope does “harden” for higher energies.

4.2. Coherence Function

The coherence function, $\gamma^2(f)$, is a frequency-dependent measure of the degree of linear correlation between two concurrent time series (Vaughan & Nowak, 1997; Nowak et al., 1999). Specifically, it gives the fraction of the variability of one time series that can be predicted from the other. The coherence is based on the Fourier transforms $S(f)$ and $H(f)$, calculated for the soft and the hard lightcurve, respectively:

$$\gamma^2(f) = \frac{|\langle S(f)^* H(f) \rangle|^2}{\langle |S(f)|^2 \rangle \langle |H(f)|^2 \rangle} \quad (1)$$

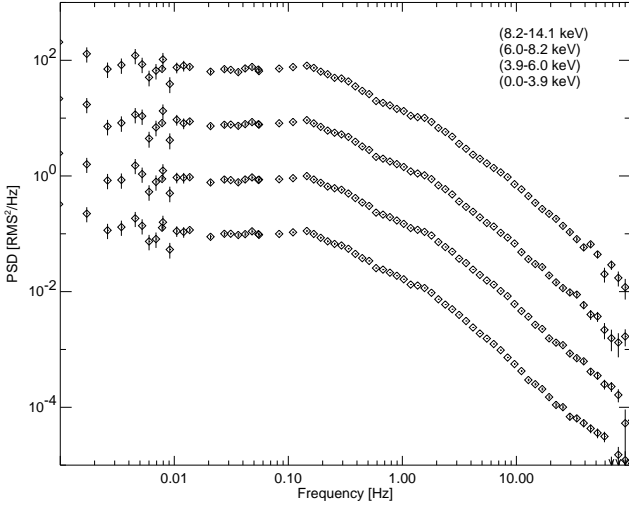


Fig. 3. Energy resolved PSDs normalized according to Miyamoto et al. (1992). PSDs for the higher energy bands have been multiplied by powers of 10 for clarity. The Poisson counting-noise has been subtracted taking the instrumental deadtime into account (Zhang et al., 1995).

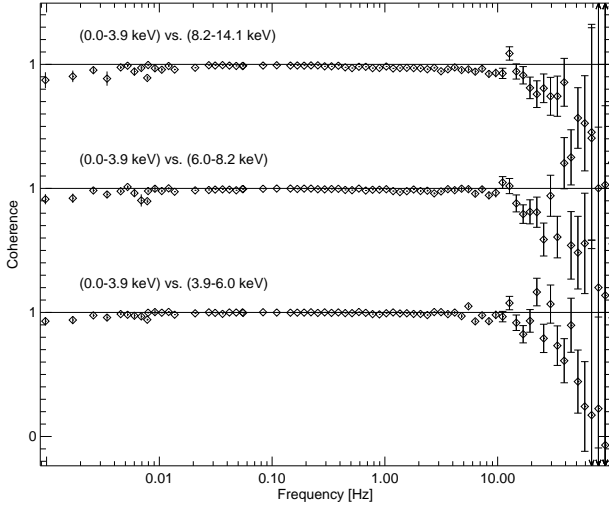


Fig. 4. Coherence between the lowest energy band and the three higher ones, corrected for Poisson counting-noise. The noise correction and the error bars have been calculated according to eq. (8) of Vaughan & Nowak (1997). Especially for high frequencies the noise-subtracted coherence is subject to additional systematic uncertainties (<30% from 30 to 100 Hz), which is why deviations to greater than unity can occur.

where the brackets indicate an average over data segments and frequency bins and the star denotes complex conjugation.

We computed the coherence function between the lowest energy band and the three higher ones using the same lightcurve segments and frequency rebinning as for the

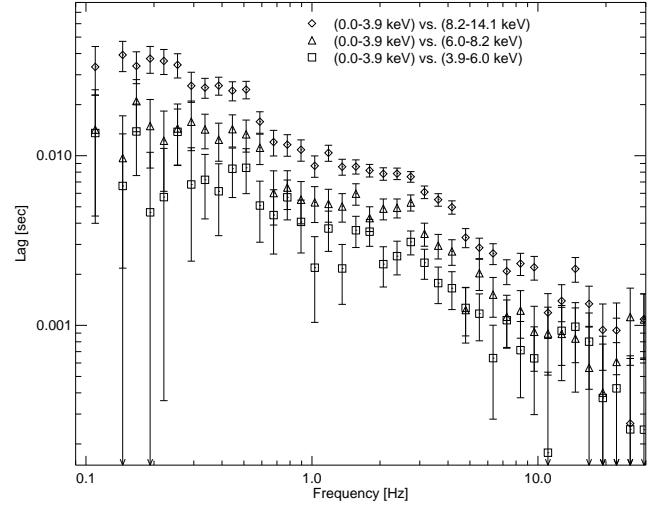


Fig. 5. Time lag as a function of frequency between the lowest energy band and the three higher ones. The error bars are calculated according to eq. (16) of Nowak et al. (1999).

PSDs. The coherence is remarkably constant and unity over the broad frequency range from 0.02 to 10 Hz (Fig. 4) – in agreement with previous results and contrary to theoretical expectations (Vaughan & Nowak, 1997; Cui et al., 1997). This behavior of γ^2 indicates that the Comptonizing medium must be static on these timescales, despite the various possibilities for non-uniform coronae (Nowak et al., 1998).

For all energy channels there is a trend for the coherence to drop below ~ 0.02 Hz and above ~ 10 Hz with the deviation from unity coherence generally becoming slightly greater for increasing energy difference. The loss of coherence below 0.02 Hz is consistent with the viscous timescale for $R > 50GM/c^2$, while the loss of coherence above 10 Hz is consistent with dynamical timescale for $R < 50GM/c^2$ (R is the distance from a $10 M_{\odot}$ black hole). For further discussion of the physical implications see Nowak et al. (1998) and Nowak et al. (1999).

4.3. Time Lags

The Fourier time lag is a frequency-dependent measure of the time delay between two time series. Like the coherence it is calculated from their Fourier transforms $S(f)$ and $H(f)$,

$$\tau(f) = \frac{\arg\langle S(f)^* H(f) \rangle}{2\pi f} \quad (2)$$

τ can be either positive or negative. For our sign convention, a positive time lag indicates that the hard lightcurve lags the soft lightcurve.

We computed the time lags for the same energy bands, lightcurve segments, and frequency bins as used for the co-

herence (Fig. 5). Within the frequency range that is not noise-dominated (0.1–30 Hz), the data are consistent with the softest energy band always leading the harder energy bands. The lags increase significantly with the energy difference between the bands and become larger for smaller frequencies, a result previously found by Miyamoto et al. (1992). The time lags range from ~ 0.002 s to ~ 0.05 s and can be very roughly described with a power law, $\tau(f) \propto f^{-0.7}$, superposed by characteristic breaks at ~ 0.5 , 3, and 10 Hz.

The simplest expectation in the framework of Comptonization models is that time delays should be due to different diffusion times through the corona and thus should be nearly independent of Fourier frequency (Miyamoto & Kitamoto, 1989). Furthermore, the overall energy dependence of the time lags is also not compatible with current Comptonization models (Nowak et al., 1999) – including the sphere+disk model. It is therefore necessary to consider more complicated accretion models (Nowak et al., 1998). The smallest observed time lags might indicate that the Comptonizing medium is rather small, $< 30 GM/c^2$. Consequently, if the time delays are due to disturbances propagating through the corona, the propagation speeds are extremely slow ($\mathcal{O}(1\text{--}10\% c)$). These values are inconsistent with current ADAF models.

5. Timing: The Linear State Space Model

An alternative method to the timing analysis in the frequency domain is to examine the X-ray variability directly in the time domain by modeling the observed lightcurves with linear state space models (LSSMs) (König & Timmer, 1997). These models describe the dynamics of a lightcurve $y(t)$ with a stochastic, autoregressive (AR) process $x(t)$ of order p (Scargle, 1981):

$$x(t) = \left(\sum_{j=1}^p a_j \cdot x(t-j) \right) + \epsilon(t) \quad (3)$$

where $\epsilon(t)$ is a Gaussian white noise processes with zero mean and variance σ_ϵ^2 . The dynamical parameters, a_j , are closely related to the temporal parameters characterizing the system. An AR[p=1] process, e.g., is described by a single relaxation timescale $\tau = -1/\ln(a_1)$.

LSSMs also take the observational noise into account. For an AR[1] process

$$y(t) = c \cdot x(t) + \eta(t) \quad (4)$$

where $\eta(t)$ is the observational noise, again given by a Gaussian white noise processes with zero mean and a variance of σ_η^2 , and where c is a constant.

We fitted LSSMs of different order to 842 contiguous lightcurve segments (0.0–14.1 keV) with a length of 16 s each. To evaluate the goodness of the fits, a Kolmogorov-Smirnov test for white noise residuals was performed. We find that the lightcurves can be modeled with a LSSM[1]

process. This is consistent with our results for modeling EXOSAT observations of Cyg X-1 (Pottschmidt et al., 1998) and in analogy to the latter work we derive a relaxation timescale $\tau = (0.13 \pm 0.03)$ s for the RXTE lightcurves. In contrast to the usually applied shot noise model fits in the frequency domain (Lochner, Swank & Szymkowiak, 1991), the LSSMs of first order do not require pre-defined shot forms and are able to describe the rapid hard state variability of Cyg X-1 with *one* temporal parameter.

The derived relaxator can in principle be used for scaling time dependent ADC models, by fitting LSSMs to theoretical “ADC lightcurves”. First estimates indicate much larger coronal radii than implied by the shortest time lags ($\sim 600 GM/c^2$). For a better understanding of spectral and temporal hard state properties in one unified accretion scenario, we plan to apply the models and methods presented here to further RXTE observations of Cyg X-1 and other BHCs.

Acknowledgements. This work has been financed by NSF grants AST91-20599, AST95-29175, INT95-13899, NASA Grant NAG5-2026, NAG5-3225, NAGS-3310, DARA grant 50 OR 92054, and by a travel grant to J.W. and K.P. from the DAAD.

References

- Belloni, T., Hasinger, G., 1990, A&A, 227, L33
 Cui, W., Zhang, S.N., Focke, W., Swank, J.H., 1997, ApJ, 484, 383
 Dove, J.B., Wilms, J., Begelman, M.C., 1997, ApJ, 487, 747
 Dove, J.B., Wilms, J., Maisack, M., Begelman, M.C., 1997, ApJ, 487, 759
 Dove, J.B., Wilms, J., Nowak, M.A., et al., 1998, MNRAS, 289, 729
 Esin, A.A., McClintock, J.E., Narayan, R., 1997, ApJ, 489, 865
 König, M., Timmer, J., 1997, A&A Suppl., 124, 589
 Lochner, J.C., Swank, J.H., Szymkowiak, A.E., 1991, ApJ, 376, 295
 Miyamoto, S., Kitamoto, S., 1989, Nature, 342, 773
 Miyamoto, S., Kitamoto, S., Iga, S., et al., 1992, ApJ, 391, L21
 Nowak, M.A., Vaughan, B.A., Wilms, J., et al., 1999, ApJ, 510, in press
 Nowak, M.A., Wilms, J., Vaughan, B.A., et al., 1998, ApJ, submitted
 Pottschmidt, K., König, M., Wilms, J., Staubert, R., 1998, A&A, 334, 201
 Scargle, J.D., 1981, ApJ Suppl., 45, 1
 Titarchuk, L., 1994, ApJ, 434, 570
 van der Klis, M., 1995, in W.H.G. Lewin, J. van Paradijs, E.P.J. van den Heuvel (eds.), X-ray Binaries, Cambridge: Univ. Cambridge Press, 252
 Vaughan, B.A., Nowak, M.A., 1997, ApJ, 474, L43
 Zhang, W., Jahoda, K., Swank, J.H., et al., 1995, ApJ, 449, 930